ISSN 0915-633X

NATIONAL INSTITUTE FOR FUSION SCIENCE

Effect of Collisionality and Radial Electric Field on Bootstrap Current in LHD (Large Helical Device)

K.Y. Watanabe, N. Nakajima, M. Okamoto, K. Yamazaki,
Y. Nakamura and M. Wakatani

(Received - May 20, 1994)

NIFS-285 June 1994

RESEARCH REPORT
NIFS Series

NAGOYA, JAPAN

Effect of Collisionality and Radial Electric Field on Bootstrap Current in LHD(Large Helical Device)

K.Y.Watanabe, N.Nakajima, M.Okamoto, K.Yamazaki

National Institute for Fusion Science,
Nagoya 464-01, Japan

Y.Nakamura, M.Wakatani

Plasma Physics Laboratory,
Kyoto University,
Gokasho, Uji, Kyoto 611, Japan

ABSTRACT

The bootstrap current reduces in more collisional regime, and in the stellarator/heliotron it is predicted that the neoclassical current proportional to radial electric field exists when electrons and ions belong to different regimes of collisionality. To evaluate the bootstrap current in stellarator/heliotron in the whole range of collisionality from the collisionless $1/\nu$ regime to the Pfirsch-Schlüter regime, a new connection formula has been proposed. We have applied this connection formula to the LHD plasmas which belongs to some collisionality regimes and obtained finite β MHD equilibria including the bootstrap current. For LHD plasmas such as ECRH ($T_i << T_e$) in electron root, the bootstrap current with electric potential twice as large as electron temperature reduces to about $1/5 \sim 2/3$ of that with zero electric potential. Then MHD equilibrium configuration significantly changes depending on collisionality and radial electric field even for the same beta value for LHD plasmas.

KEYWORDS : bootstrap current, stellarator, heliotron, neoclassical current, collisionality, radial electric field, MHD equilibrium

1. INTRODUCTION

The neoclassical theory for helical systems predicts the existence of the bootstrap current particularly in collisionless plasmas[1]. In several helical system such as ATF[2], WVII-AS[3] and CHS[4], the experimental evidence of bootstrap current has been obtained and measured currents agree reasonably with the theoretical estimation based on the neoclassical theory. The bootstrap current is supposed to be crucial for the shearless system such as WVII-AS, on the other hand, it is not dangerous for heliotron/torsatron with the finite magnetic shear such as LHD(Large Helical Devices)[5] from the view point of the MHD equilibria and stabilities. To check this speculation, we already studied the effect of bootstrap current on the finite β MHD equilibrium including bootstrap current under the assumption that both ions and electrons belong to the same collisionless regime ($1/\nu$ regime)[6]. It is demonstrated that, even in heliotron/torsatron with the finite magnetic shear, the bootstrap current is very important to evaluate property of MHD equilibria since in LHD 'standard configuration', the bootstrap current enhances the rotational transform and reduces Shafranov shift. The reduction of Shafranov shift leads to the unfavorable effect on the MHD stabilities through the change of magnetic well[7].

The magnitude of bootstrap current is influenced by the magnetic configuration, the density and temperature profiles, the collisionality and so on. The collisionality is determined by the ripple of magnetic field strength, the density and the temperature. Thus, the precise evaluation of bootstrap current needs the proper treatment of the collisionality. Moreover, in the asymmetric toroidal system, it is predicted that the neoclassical current has the component proportional to radial electric field, E_ψ, when electrons and ions belong to different collisionality regimes[8,9]. Here our main concern is the collisionality and the radial electric field effects on the bootstrap current and the consistent MHD equilibria. The parallel viscosities of the neoclassical theory are described using the thermodynamic forces, the parallel flows, the viscosity coefficients and the geometric factors shown in Appendix A. The viscosity coefficients and the geometric factors determine the magnitude and the direction of plasma flow to be damped. In asymmetric toroidal plasmas, the direction of the flow damped by the parallel viscosities depends on the particle species through their collisionalities due to the lack of symmetry. This fact is reflected on the collisionality dependence of the geometric factor. When ions and electrons exist in well separated collisionality regimes, the direction of plasma flow of each particle species damped by the parallel viscosities, *i.e.* the geometric factor, is different, which makes the different parallel flow proportional to E_ψ and leads to the neoclassical current proportional to E_ψ. On the other hand, in the symmetric toroidal plasmas, the direction of the flow damped by the parallel viscosities is determined by the symmetry

and is independent of the particle species, which is reflected on the fact that the geometric factor of all the particle species is the same. Thus, the neoclassical current proportional to E_ψ vanishes, since the total momentum of the system is conserved.

In order to estimate the collisionality and the radial electric field dependence of the bootstrap current, we have proposed a connection formula for bootstrap current in stellarator/heliotron which is usable in the whole collisionality regimes from $1/\nu$ to Pfirsch-Schlüter (P-S) regime. So far, for stellarator/heliotron, such a connection formula does not exist, but only the asymptotic expressions exist for each collisionality regime in the Hamada coordinates[1,10]. We have connected the asymptotic expressions in each collisionality regime using the similar technique to the Hirshman and Sigmer[11] and in the Boozer coordinates which is suitable for numerical calculations. We have applied this connection formula to the LHD plasmas which belong to some collisionality regimes and obtained the finite β MHD equilibria including the bootstrap current.

This paper is organized in the following way. In Section 2, the connection formula for bootstrap current is described, which is usable in the whole range of collisionality from $1/\nu$ to P-S regimes. In Section 3, the effect of the collisionality on the bootstrap current and the MHD equilibrium for the case that ions and electrons belong to the same collisionality regime is studied. In Section 4, the effect of the radial electric field is shown in the case that the neoclassical current proportional to E_ψ is not negligible. In Section 5 obtained results are discussed. The connection formula for the parallel viscosity, plasma flow and the geometric factor in the plateau and P-S collisionality regimes in the Boozer coordinates are described in Appendix A and B.

2. CONNECTION FORMULA

We have constructed a connection formula for bootstrap current in asymmetric system which is available in the whole range of collisionality from $1/\nu$ to P-S regimes according to Hirshman and Sigmer[11]. The bootstrap current in the plasma consisting of primary ions and electrons is written as

$$\langle j_{bs} B \rangle = L_{1e}\left(\frac{\mathrm{d}P_e}{\mathrm{d}\psi} + e n_e E_\psi\right) + L_{1i}\left(\frac{\mathrm{d}P_i}{\mathrm{d}\psi} - e n_e E_\psi\right) - L_{2e} n_e \frac{\mathrm{d}T_e}{\mathrm{d}\psi} + L_{2i} n_e \frac{\mathrm{d}T_i}{\mathrm{d}\psi}, \tag{1}$$

where

$$L_{1e} = \frac{(\mu_{e3} - \bar{l}_{22}^{ee})\langle \mu G_{bs} \rangle_{e1} - (\mu_{e2} - \bar{l}_{12}^{ee})\langle \mu G_{bs} \rangle_{e2}}{D_e}, \tag{2}$$

$$L_{1i} = \frac{\mu_{e1}(\mu_{e3} - \bar{l}_{22}^{ee}) - \mu_{e2}(\mu_{e2} - \bar{l}_{12}^{ee})}{D_e} \cdot F_g, \tag{3}$$

$$F_g = \frac{(\mu_{i3} - \bar{l}_{22}^{ii})\langle \mu G_{bs}\rangle_{i1} - \mu_{i2}\langle \mu G_{bs}\rangle_{i2}}{D_i}, \tag{4}$$

$$L_{2e} = \frac{-(\mu_{e3} - \bar{l}_{22}^{ee})\langle \mu G_{bs}\rangle_{e2} + (\mu_{e2} - \bar{l}_{12}^{ee})\langle \mu G_{bs}\rangle_{e3}}{D_e}, \tag{5}$$

$$L_{2i} = \frac{\mu_{e1}(\mu_{e3} - \bar{l}_{22}^{ee}) - \mu_{e2}(\mu_{e2} - \bar{l}_{12}^{ee})}{D_e} \cdot G_g, \tag{6}$$

$$G_g = \frac{-(\mu_{i3} - \bar{l}_{22}^{ii})\langle \mu G_{bs}\rangle_{i2} + \mu_{i2}\langle \mu G_{bs}\rangle_{i3}}{D_i}, \tag{7}$$

$$D_e = (\mu_{e1} - \bar{l}_{11}^{ee})(\mu_{e3} - \bar{l}_{22}^{ee}) - (\mu_{e2} - \bar{l}_{12}^{ee})^2, \tag{8}$$

$$D_i = \mu_{i1}(\mu_{i3} - \bar{l}_{22}^{ii}) - \mu_{i2}^2. \tag{9}$$

Here j_{bs} is the bootstrap current density, B is the magnitude of magnetic field and $\langle\ \rangle$ means the flux surface average. n_e, n_i, T_e and T_i are electron density, ion density, electron temperature and ion temperature, respectively. P is the total pressure, $P = n_eT_e + n_iT_i$. $\psi \equiv \Phi_T/2\pi$, where Φ_T is the toroidal flux. $\bar{l}_{ij}^{ab}$ are the friction coefficients between species a and b. By neglecting terms of $O(m_e/m_i)$, $\bar{l}_{11}^{ee} = Z$, $\bar{l}_{12}^{ee} = \frac{3}{2}Z$, $\bar{l}_{22}^{ee} = \sqrt{2} + \frac{13}{4}Z$, and $\bar{l}_{22}^{ee} = \sqrt{2}$. Here Z is the effective ionic charge number. We assume $Z = 1$ in this paper. μ_{aj} and $\langle \mu G_{bs}\rangle_{aj}/\mu_{aj}$ denote the viscosity coefficient and the geometric factors, and depend on the collisionality. In Ref.[11], the viscosity coefficients are smoothly interpolated from the banana to P-S regimes for the axisymmetric tokamak. In asymmetric system, we should connect the geometric factors as well as the viscosity coefficients because both the geometric factors and the viscosity coefficient depend on the collisionality. We connect the viscosity coefficients and the geometric factors as following by extending the way of Ref.[11],

$$\mu_{a1} = K_{11}^a, \quad \mu_{a2} = -K_{12}^a + \frac{5}{2}K_{11}^a, \quad \mu_{a3} = K_{22}^a - 5K_{12}^a + \frac{25}{4}K_{11}^a, \tag{10}$$

$$\langle \mu G_{bs}\rangle_{a1} = \bar{K}_{11}^a, \quad \langle \mu G_{bs}\rangle_{a2} = -\bar{K}_{12}^a + \frac{5}{2}\bar{K}_{11}^a, \quad \langle \mu G_{bs}\rangle_{a3} = \bar{K}_{22}^a - 5\bar{K}_{12}^a + \frac{25}{4}\bar{K}_{11}^a, \tag{11}$$

$$K_{ij}^a \equiv \frac{8}{3\sqrt{\pi}}\frac{f_t}{f_c}\int_0^\infty \exp(-x_a^2)x_a^{2(i+j)}[[\nu_{tot}^a(x_a)/\nu_a]]\mathrm{d}x_a, \tag{12}$$

$$\bar{K}_{ij}^a \equiv \frac{8}{3\sqrt{\pi}}\frac{f_t}{f_c}\int_0^\infty \exp(-x_a^2)x_a^{2(i+j)}[[G_{bs}\nu_{tot}^a(x_a)/\nu_a]]\mathrm{d}x_a, \tag{13}$$

$$x_a = \frac{v}{v_{ta}}, \tag{14}$$

where

$$[[\nu_{tot}^a(x_a)/\nu_a]] \equiv \frac{\bar{\nu}_D^a(x_a)}{(1 + \bar{\nu}_{*a}\frac{\bar{\nu}_D^a}{x_a})(1 + \frac{5\pi}{8}\frac{\bar{\nu}_T^a}{x_a}\frac{1}{\bar{\omega}_{ta}})}, \tag{15}$$

$$[[G_{bs}\nu^a_{tot}(x_a)/\nu_a]] \equiv \frac{\bar{\nu}^a_D(x_a)}{(1+\bar{\nu}_{*a}\frac{\bar{\nu}^a_D}{x_a})^2(1+\frac{5\pi}{8}\frac{\bar{\nu}^a_T}{x_a}\frac{1}{\bar{\omega}_{ta}})^2}$$
$$\times\{\langle G_{bs}\rangle^{1/\nu}_a + (\bar{\nu}_{*a}\frac{\bar{\nu}^a_D}{x_a} + \frac{5\pi}{8}\frac{\bar{\nu}^a_T}{x_a}\frac{1}{\bar{\omega}_{ta}})\langle G_{bs}\rangle^{pl}_a + \frac{5\pi}{8}\bar{\nu}_{*a}\frac{\bar{\nu}^a_D}{x_a}\frac{\bar{\nu}^a_T}{x_a}\frac{1}{\bar{\omega}_{ta}}\langle G_{bs}\rangle^{PS}_a\}, \tag{16}$$

$$\bar{\nu}^a_D = \nu^a_D(x_a)/\nu_a, \quad \bar{\nu}^a_T = \nu^a_T(x_a)/\nu_a. \tag{17}$$

Here $\nu^a_T(x_a) = 3\nu^a_D(x_a) + \nu^a_E(x_a)$, ν^a_D and ν^a_E are the 90° deflection frequency and the energy exchange frequency, respectively. The normalized transit frequency $\bar{\omega}_{ta}$, which corresponds to the boundary between the plateau and P-S collisionality regimes, is given by

$$\bar{\omega}_{ta} \equiv \frac{\lambda_a}{L^*_c} = \frac{\sqrt{\pi}}{3}\frac{\lambda_{pl}\lambda_a}{\lambda^2_{PS}}, \tag{18}$$

where L^*_c is the effective connection length and

$$L^*_c = \frac{3}{\sqrt{\pi}}\frac{\lambda^2_{PS}}{\lambda_{pl}}. \tag{19}$$

And the normalized collision frequency $\bar{\nu}_{*a}$, which corresponds to the boundary between the $1/\nu$ and plateau collisionality regimes, is given by

$$\bar{\nu}_{*a} \equiv \frac{8}{3\pi}\frac{f_t}{f_c}\frac{\langle B^2\rangle}{\lambda^2_a\langle(\hat{n}\cdot\nabla B)^2\rangle}\bar{\omega}_{ta} = \frac{4}{3\sqrt{\pi}}\frac{f_t}{f_c}\frac{\lambda_{pl}}{\lambda_a}, \tag{20}$$

where $\bar{\omega}_{ba} = 1/\bar{\nu}_{*a}$ is the normalized bounce frequency. Here f_c is the fraction of untrapped particles and $f_t = 1 - f_c$. And v_{ta} and ν_a are the thermal velocity and the collision frequency for the particles with thermal velocity, respectively. $\lambda_a = v_{ta}/\nu_a$ is the mean free path. λ_{pl} and λ_{PS} are the characteristic length of the magnetic field inhomogeneity in the plateau and P-S collisionality regimes, respectively, which are described in Appendix B. It is noticed that $\bar{\nu}_{*a} << 1$ corresponds to the $1/\nu$-regime limit, $\bar{\nu}_{*a} >> 1$ and $\bar{\nu}_{*a}/\bar{\omega}_{ta} << 1$ to the plateau regime limit, and $\bar{\nu}_{*a}/\bar{\omega}_{ta} >> 1$ to the P-S regime limit. $\langle G_{bs}\rangle^{1/\nu}$, $\langle G_{bs}\rangle^{pl}$ and $\langle G_{bs}\rangle^{PS}$ are the geometric factors for the $1/\nu$, plateau and P-S collisionality regimes, respectively[10,12]. For the asymmetric system, the difference of collisionality dependence between ions and electrons of $\langle\mu G_{bs}\rangle_{aj}/\mu_{aj}$ leads to the appearance of the neoclassical current proportional to E_ψ. In this case $L_{1e} \neq L_{1i}$ because the collisionality of ion is not same as that of electron. When both ions and electrons belong to the same collisionalities in the asymmetric system, the neoclassical current proportional to E_ψ is small because $\langle\mu G_{bs}\rangle_{ij}/\mu_{ij} \simeq \langle\mu G_{bs}\rangle_{ej}/\mu_{ej}$ and $L_{1e} \simeq L_{1i}$. On the other hand, the geometric factor is independent of collisionality in the axisymmetric system, *i.e.*, $\langle\mu G_{bs}\rangle_{aj}/\mu_{aj} = I_p/2\pi\iota$, where I_p is the poloidal current outside the flux surface

and ι is the rotational transform. Thus, the current proportional to E_ψ vanishes in the axisymmetric system.

For $\langle \vec{j} \cdot \vec{B} \rangle \neq 0$, the total toroidal current inside the flux surface $I_T(\psi)$ is given by

$$I_T(\psi) = 2\pi \int \mathrm{d}\psi \frac{\langle \vec{j} \cdot \vec{B} \rangle}{\langle B^2 \rangle} - \int \mathrm{d}\psi \frac{\mathrm{d}P}{\mathrm{d}\psi} \frac{I_T}{\langle B^2 \rangle}. \tag{21}$$

The second term in the right hand side comes from the diamagnetic current and this is small for the low β plasma. In this paper, we ignore this term and take only bootstrap current into account as the flux surface averaged parallel current, $I_T = 2\pi \int \mathrm{d}\langle j_{bs} B \rangle / B^2$[6]. Here a self-consistent equilibrium solution is obtained by calculating j_{bs} and the finite β MHD equilibrium including j_{bs} iteratively. We employ the VMEC code[13,14] in order to obtain the three-dimensional MHD equilibrium with the net plasma current. And we assume the fixed boundary condition in the finite β MHD equilibrium calculation.

3. EFFECT OF COLLISIONALITY

We have applied the connection formula for bootstrap current Eq.(1) to the LHD plasmas with the standard configuration ($L = 2$, $M = 10$, $R_C = 3.9$m, $B_0 = 3$T $\alpha = 0.1$ $R_{ax}^V = 3.75$m and $B_Q = 100\%$, where L and M are the pole number and the toroidal pitch number of the helical coil, R_C is the major radius at the axis of the helical coil. B_0 is the magnitude of the magnetic field, α is the pitch modulation parameter, R_{ax}^V is the major radius of the vacuum magnetic axis and B_Q is the quadrupole field produced by the axisymmetric poloidal coils which is added to the quadrupole field by the helical coil)[15].

At first, we consider the case that both ions and electrons belong to the almost same collisionality regime ($T_i \simeq T_e$). In this case, the neoclassical current proportional to E_ψ is very small. Figures 1 and 2 show the radial profile of bootstrap current density and collisionality parameter, $\bar{\nu}^*$ for different collisionality (or density) with the same β value, $\langle \beta \rangle \simeq 1.5\%$. $s = \psi/\psi_{edge}$. Here $\bar{\nu}_i^* = \bar{\nu}_e^* \equiv \bar{\nu}^*$ since $T_i = T_e$, and $\bar{\nu}^* << 1$ and $\bar{\nu}^* >> 1$ correspond to the $1/\nu$-regime limit and the plateau-regime limit, respectively. In Figs.1(a) and 2(a), solid lines correspond to the connection formula Eq.(1). Dashed lines and dotted-dashed lines correspond to the cases assuming the $1/\nu$-regime limit and the plateau-regime limit, respectively. Figure 1 corresponds to the low collisionality regime (or low density case of $\langle n \rangle = 0.25 \times 10^{20}\mathrm{m}^{-3}$). In this case, both ions and electrons in the whole plasma region belong to the $1/\nu$-regime completely. Thus the bootstrap current density evaluated by the connection formula Eq.(1) is very closed to evaluated with assumption that both ions and electrons in the whole plasma region belong to the $1/\nu$-regime limit. Figure 2 corresponds to the high collisionality regime (or high density

case of $\langle n \rangle = 2.0 \times 10^{20}\mathrm{m}^{-3}$). In this case, both ions and electrons in the whole plasma region belong to the plateau-regime. Thus the bootstrap current density evaluated by the connection formula Eq.(1) is significantly reduced comparing with that assuming the $1/\nu$-regime limit. Here it should be noted that $\bar{\nu}^*$ is estimated by the thermal speed and that the contribution of high energy particles to the bootstrap current is large in our connection formula Eq.(1).

Figure 3 show the dependence of (a) the total bootstrap current and (b) the collisionality parameter $\bar{\nu}^*$ at $\sqrt{s} \simeq 0.7$ for several density (or collisionality) case as a function of central beta value,β_0 . Circles, triangles and squares correspond to $\langle n \rangle = 0.25 \times 10^{20}\mathrm{m}^{-3}$, $\langle n \rangle = 1.0 \times 10^{20}\mathrm{m}^{-3}$ and $\langle n \rangle = 2.0 \times 10^{20}\mathrm{m}^{-3}$, respectively. The density and temperature profiles are assumed as $n = n_0(1-s)$ and $T_i = T_e = T_0(1-s)$. Then $\langle \beta \rangle = \beta_0/3$. According to our connection formula, the total bootstrap current in the case that ions and electrons belong to the plateau-P-S regime, $\bar{\nu}^* > 10^1$, is smaller than in the $1/\nu$-regime, $\bar{\nu}^* < 10^{-1}$ by $1/10$ (squares at and circles at $\beta_0 \simeq 2\%$ in Fig.3). In more collisional case that ions and electrons belong to the plateau-regime, $\bar{\nu}^* > 3$, the total bootstrap current is nearly $1/3$ of that in the deep $1/\nu$-regime, $\bar{\nu}^* < 10^{-1}$ (squares and circles at $\beta_0 \simeq 4.5\%$ in Fig.3). Figure 4 shows the dependence of magnetic axis position on β value for various density (or collisionality) cases. Circles and squares correspond to $\langle n \rangle = 0.25 \times 10^{20}\mathrm{m}^{-3}$ and $\langle n \rangle = 2.0 \times 10^{20}\mathrm{m}^{-3}$, respectively. Rhombuses correspond to the currentless MHD equilibrium. Other parameters are the same as in Fig.3. Even in the high density case of $\langle n \rangle = 2.0 \times 10^{20}\mathrm{m}^{-3}$ at $\langle \beta \rangle \simeq 1.5\%$ the Shafranov shift calculated by the equilibrium with bootstrap current is reduced to about 20% of that obtained using currentless MHD equilibrium. And in the high density case ($\langle n \rangle = 2.0 \times 10^{20}\mathrm{m}^{-3}$), the Shafranov shift is twice larger and the change of central rotational transform is $1/5$ times smaller than those in the low density case ($\langle n \rangle = 0.25 \times 10^{20}\mathrm{m}^{-3}$). Figures 5 and 6 show rotational transform profile and magnetic well depth parameter in (a) currentless case, (b) low density case of $\langle n \rangle = 0.25 \times 10^{20}\mathrm{m}^{-3}$ and (c) high density case of $\langle n \rangle = 2.0 \times 10^{20}\mathrm{m}^{-3}$ at various β value. These results in Figs.5 and 6 correspond to Fig.4. In the low density case (b), rotational transform ι in the whole plasma region increases with β by the bootstrap current, which leads to the reduction of the Shafranov shift and the magnetic well. In the high density case (c), at low β, ι and well depth behave like the currentless case. However, for rather high β with over 50kA bootstrap current, the bootstrap current effects on the reduction of the Shafranov shift and the magnetic well become significantly large comparing with currentless case, which leads to unfavorable effect on the ideal interchange instability[7].

4. EFFECT OF RADIAL ELECTRIC FIELD

In the case that ions and electrons belong to the different collisionality regimes

($T_i \neq T_e$), the neoclassical current proportional to E_ψ does not varnish in stellarator/heliotron and this effect becomes important to evaluate MHD equilibria. The direction and amplitude of the neoclassical current depend on the collisionality of the ions and electrons, and the direction and amplitude of radial electric field. In ECH case ($T_e >> T_i$), the ions and electrons are supposed to belong to the plateau and $1/\nu$ regimes. For the LHD standard configuration, electron root ($E_\psi > 0$) leads to the reduction of the bootstrap current, and ion root ($E_\psi < 0$) to the increase of the bootstrap current. Figure 7 shows the dependence of the total bootstrap current on β value for various E_ψ. Circles, triangles and squares correspond to $\Phi = 0$, $\Phi = T_e$ and $\Phi = 2T_e$, respectively. Here $E_\psi = -\mathrm{d}\Phi/\mathrm{d}\psi$. We assume that the density and temperature profiles are $n = n_0(1-s)$ and $4T_i = T_e = T_0(1-s)$, where $\langle n \rangle$ is fixed at $1.0 \times 10^{20}\mathrm{m}^{-3}$. The dependence of collisionality parameter $\bar{\nu}^*$ at $\sqrt{s} \simeq 0.7$ on β value is shown in Fig.8. Open circles and closed ones correspond to ion and electron collisionality parameters $\bar{\nu}_i^*$ and $\bar{\nu}_e^*$ in Fig.7, respectively. For $\langle n \rangle = 1.0 \times 10^{20}\mathrm{m}^{-3}$ and $T_i : T_e = 1 : 4$, $\nu_{*i}/\nu_{*e} \simeq 10^1$. The neoclassical current proportional to E_ψ is not so large comparing with the bootstrap current due to small difference between the ion and electron collisionalities. Even for $\Phi_0 = 2T_{e0}$, the neoclassical current is nearly 1/3 of the bootstrap current in the case that $\langle n \rangle = 1.0 \times 10^{20}\mathrm{m}^{-3}$ and $\beta_0 \simeq 1.5\%$.

Figure 9(a) shows the dependence of the total bootstrap current on radial electric field at the fixed beta value $\langle \beta \rangle \simeq 1.5\%$. Circles and squares correspond to the case of $T_{i0} = 1.0\mathrm{keV}$, $T_{e0} = 4.0\mathrm{keV}$ (small difference case between electron and ion collisionalities) and the case of $T_{i0} = 0.5\mathrm{keV}$, $T_{e0} = 4.5\mathrm{keV}$ (large difference case between electron and ion collisionalities) at $\langle n \rangle = 1.0 \times 10^{20}\mathrm{m}^{-3}$, respectively. Here $\Phi_0 > 0$ and $\Phi_0 < 0$ correspond to $E_\psi > 0$ and $E_\psi < 0$, respectively. It is noted that open square and closed one correspond to ion and electron collisionality parameter for the case of $T_{i0} = 0.5\mathrm{keV}$, $T_{e0} = 4.5\mathrm{keV}$, $\langle n \rangle = 1.0 \times 10^{20}\mathrm{m}^{-3}$ in Fig.6, respectively. In this case, $\nu_{*i}/\nu_{*e} \simeq 10^2$ and ion belong to the plateau regime completely. Then the neoclassical current proportional to E_ψ becomes large and for $\beta_0 \simeq 4.5\%$, $\Phi_0 = 2T_{e0}$ the neoclassical current is about 80% of the bootstrap current. In this case, the Shafranov shift is twice larger than that in the $E_\psi = 0$ case as shown in Fig.9(b), which shows dependence of magnetic axis position on radial electric field for $\langle \beta \rangle \simeq 1.5\%$. It is noted that in Fig.9(b) dashed-dotted line corresponds to the currentless MHD equilibrium. Figure 10 shows the rotational transform profile for the cases of $T_{i0} = 1.0\mathrm{keV}$, $T_{e0} = 4.0\mathrm{keV}$ (small difference case between electron and ion collisionalities) and $T_{i0} = 0.5\mathrm{keV}$, $T_{e0} = 4.5\mathrm{keV}$ (large difference case between electron and ion collisionalities) for $\langle n \rangle = 1.0 \times 10^{20}\mathrm{m}^{-3}$. From these figures, we can expect that the MHD equilibrium of LHD is affected significantly by the radial electric field through the bootstrap current especially for the large difference case between

electron and ion collisionalities.

5. CONCLUDING REMARKS

The magnitude of bootstrap current is influenced by the magnetic configuration, the density and the temperature profile, collisionality and so on. In this paper, we study the effect of collisionality and radial electric field on bootstrap current. It is expected that bootstrap current reduces in more collisional regime. In the stellarator/heliotron, it is predicted that the neoclassical current proportional to radial electric field exists when electrons and ions belong to different regimes of collisionality. It is noticed that in the systems with symmetry the angular momentum conserves, the neoclassical current proportional to radial electric field varnishes, and in the systems without symmetry and with the same collisionalities of ion and electron, the above neoclassical current is small.

The connection formula for the bootstrap current usable in the whole range of collisionality from the collisionless $1/\nu$ regime to the P-S regime has been given based on the idea that the asymptotic distribution functions of each collisionality regime are connected in the velocity space. We have applied this connection formula to the LHD plasmas which belongs to some collisionality regimes, and obtained the finite β MHD equilibria including the bootstrap current. In the LHD plasmas at $B_0 = 3T$, we obtain the following results.

[CASE 1] Ions and electrons belong to the almost same collisionality regime ($T_i \simeq T_e$).

The neoclassical current proportional to radial electric field is very small. Even for the same $\langle\beta\rangle$ case ($\langle\beta\rangle \simeq 1.5\%$), the total bootstrap current in the high density case ($\langle n\rangle = 2.0 \times 10^{20}\mathrm{m}^{-3}$) is nearly 1/3 of that in the low density case ($\langle n\rangle = 0.25 \times 10^{20}\mathrm{m}^{-3}$), and the Shafranov shift is about twice and the variation of central rotational transform is nearly 1/5. It is noted that the ions and electrons in the whole plasma region belong to the $1/\nu$-regime completely in the low density case, and to the plateau-regime mostly in the high density case.

[CASE 2] Ions and electrons belong to the different collisionality regime ($T_i \neq T_e$).

The effect of the neoclassical current proportional to radial electric field becomes large. The direction and amplitude of above neoclassical current depend on the ion and electron collisionalities, and the sign and amplitude of radial electric field. Supposed the ions and electrons belong to the plateau and $1/\nu$-regime, respectively. This situation would be likely to be realized in ECH plasmas with $T_e >> T_i$. Electron root ($E_r > 0$) and ion root ($E_r < 0$) correspond to the reduction and emphasis of the bootstrap current, respectively, for the LHD standard configuration. For $\langle\beta\rangle \simeq 1.5\%$, $\langle n\rangle = 1.0 \times 10^{20}\mathrm{m}^{-3}$

and $T_i = (1/4)T_e$, the positive radial electric field ($\Phi = 2T_e$ case) reduces total bootstrap current to about 2/3. And in large difference case between ion and electron collisionalities ($T_{i0} = 0.5$keV, $T_{e0} = 4.5$keV) with $\Phi = 2T_e$, the bootstrap current reduces to nearly 1/5 comparing with $E_\psi = 0$.

In the LHD plasmas, the collisionality affects significantly the bootstrap current and the MHD equilibria. Even in the same β value, different density (or temperature) and E_ψ lead to different MHD equilibria. Thus, it is important to taking account into the effect of collisionality and radial electric field on bootstrap current in comparing experimental results with the theory.

ACKNOWLEDGEMENTS

We acknowledge Dr S. P. Hirshman for permitting to use the VMEC code.

Appendix A. CONNECTION FORMULA FOR PARALLEL VISCOSITIES AND FLOWS

The parallel momentum viscosity and the parallel heat viscosity for the collisionality regimes from the $1/\nu$ to P-S regimes are written as

$$\begin{aligned}
&\begin{bmatrix} \langle \vec{B}\cdot\nabla\cdot\Pi_a\rangle \\ -\langle \vec{B}\cdot\nabla\cdot\Theta_a\rangle \end{bmatrix} \\
&= n_a m_a \nu_a \begin{bmatrix} \mu_{a1} & \mu_{a2} \\ \mu_{a2} & \mu_{a3} \end{bmatrix} \begin{bmatrix} \langle u_{\|a} B\rangle \\ -\frac{2}{5}\frac{\langle q_{\|a} B\rangle}{P_a} \end{bmatrix} \\
&+ n_a m_a \nu_a \begin{bmatrix} \langle \mu G_{bs}\rangle_{a1} & \langle \mu G_{bs}\rangle_{a2} \\ \langle \mu G_{bs}\rangle_{a2} & \langle \mu G_{bs}\rangle_{a3} \end{bmatrix} \begin{bmatrix} \frac{T_a}{e_a}\left(\frac{1}{P_a}\frac{\mathrm{d}P_a}{\mathrm{d}\psi} + \frac{e_a}{T_a}\frac{\mathrm{d}\Phi}{\mathrm{d}\psi}\right) \\ -\frac{1}{e_a}\frac{\mathrm{d}T_a}{\mathrm{d}\psi} \end{bmatrix}, \qquad \text{(A.1)} \\
&= n_a m_a \nu_a \begin{bmatrix} \frac{I_T}{2\pi}\mu_{a1} + \langle \mu G_{bs}\rangle_{a1} & \frac{I_T}{2\pi}\mu_{a2} + \langle \mu G_{bs}\rangle_{a2} \\ \frac{I_T}{2\pi}\mu_{a2} + \langle \mu G_{bs}\rangle_{a2} & \frac{I_T}{2\pi}\mu_{a3} + \langle \mu G_{bs}\rangle_{a3} \end{bmatrix} \begin{bmatrix} \langle \vec{u}_a\cdot\nabla\theta_B\rangle \\ -\frac{2}{5}\frac{\langle \vec{q}_a\cdot\nabla\theta_B\rangle}{P_a} \end{bmatrix} \\
&+ n_a m_a \nu_a \begin{bmatrix} \frac{I_P}{2\pi}\mu_{a1} - \iota\langle \mu G_{bs}\rangle_{a1} & \frac{I_P}{2\pi}\mu_{a2} - \iota\langle \mu G_{bs}\rangle_{a2} \\ \frac{I_P}{2\pi}\mu_{a2} - \iota\langle \mu G_{bs}\rangle_{a2} & \frac{I_P}{2\pi}\mu_{a3} - \iota\langle \mu G_{bs}\rangle_{a3} \end{bmatrix} \begin{bmatrix} \langle \vec{u}_a\cdot\nabla\zeta_B\rangle \\ -\frac{2}{5}\frac{\langle \vec{q}_a\cdot\nabla\zeta_B\rangle}{P_a} \end{bmatrix}, \qquad \text{(A.2)}
\end{aligned}$$

using the connection formula for the viscosities and geometric factors, μ_{aj} and $\langle \mu G_{bs}\rangle_{aj}$, in Section 2. It is noted that for toroidally symmetric systems, $\langle \mu B_{bs}\rangle_{aj} = (I_P/2\pi)\mu_{aj}$ and that for poloidally symmetric systems, $\langle \mu B_{bs}\rangle_{aj} = -(I_T/2\pi)\mu_{aj}$. Then, for such symmetric systems, the directions of plasma flows to be damped become the same for

all species regardless of their collisionalities since the geometric factors are changed in such a way that parallel viscosity damps the flow in the direction with no symmetry. For symmetric systems, the direction of the flow damping does not depend on the collisionalities and only the magnitude of damping depends on the collisionalities. On the other hand, for asymmetric systems, the magnitude of damping the flows as well as the direction depend on the collisionalities[9].

Substituting the relationships between the parallel flows and the frictions and (A.1) into the parallel momentum and heat flux balance equation, we can obtain the following flux-surface averaged parallel flows for ions and electrons:

$$\begin{aligned}\langle u_{\|e}B\rangle &= L_{1e}\frac{1}{en_e}\frac{\mathrm{d}P_e}{\mathrm{d}\psi}+(L_{1i}-F_g)\frac{1}{en_e}\frac{\mathrm{d}P_i}{\mathrm{d}\psi}+(-L_{1e}+L_{1i}-F_g)\frac{\mathrm{d}\Phi}{\mathrm{d}\psi}\\ &\quad +L_{2e}\frac{1}{e}\frac{\mathrm{d}T_e}{\mathrm{d}\psi}+(L_{2i}-G_g)\frac{1}{Ze}\frac{\mathrm{d}T_i}{\mathrm{d}\psi}-\frac{\sigma_{NC}}{en_e}\langle BE_{\|}^{(A)}\rangle, \qquad (A.3)\\ \langle u_{\|i}B\rangle &= -F_g\left(\frac{1}{en_e}\frac{\mathrm{d}P_i}{\mathrm{d}\psi}+\frac{\mathrm{d}\Phi}{\mathrm{d}\psi}\right)-G_g\frac{1}{Ze}\frac{\mathrm{d}T_i}{\mathrm{d}\psi}, \qquad (A.4)\\ \sigma_{NC} &= \frac{e^2n_e}{m_e\nu_e}\frac{Z(\mu_{e3})-\bar{l}_{22}^{ee}}{D_e}. \qquad (A.5)\end{aligned}$$

Appendix B. GEOMETRIC FACTOR AND CHARACTERISTIC LENGTH OF MAGNETIC FIELD INHOMOGENEITY IN PLATEAU AND P-S COLLISIONAL REGIME IN BOOZER COORDINATES

The geometric factors and the characteristic lengths of the magnetic field inhomogeneity in the plateau and P-S collisionality regimes are given in Boozer coordinates (ψ, θ_B, ζ_B)[10,16],

$$\langle G_{bs}\rangle^{pl} = \frac{\langle(\hat{n}\cdot\nabla B)\sum_{mn}\frac{1}{|n+\iota m|}[\frac{1}{2B}(\frac{\partial}{\partial\theta_B}+\iota\frac{\partial}{\partial\zeta_B})(B^2\langle g_2\rangle-\langle B^2\rangle g_2)]_{mn}\exp\{\mathrm{i}(m\theta_B+n\zeta_B)\}\rangle}{\langle(\hat{n}\cdot\nabla B)\sum_{mn}\frac{1}{|n+\iota m|}[(\frac{\partial}{\partial\theta_B}+\iota\frac{\partial}{\partial\zeta_B})]_{mn}\exp\{\mathrm{i}(m\theta_B+n\zeta_B)\}\rangle}, \qquad (B.1)$$

$$\frac{1}{\lambda_{pl}} = \frac{\sqrt{\pi}}{\langle B^2\rangle}\langle(\hat{n}\cdot\nabla B)\sum_{mn}\frac{1}{|n+\iota m|}[(\frac{\partial}{\partial\theta_B}+\iota\frac{\partial}{\partial\zeta_B})B]_{mn}\exp\{\mathrm{i}(\mathrm{m}\theta_\mathrm{B}+\mathrm{n}\zeta_\mathrm{B})\}\rangle, \qquad (B.2)$$

$$\langle G_{bs}\rangle^{PS} = \frac{\langle(\hat{n}\cdot\nabla B)\frac{1}{2B}\hat{n}\cdot\nabla(B^2\langle g_2\rangle-\langle B^2\rangle g_2)\rangle}{\langle(\hat{n}\cdot\nabla B)^2\rangle}, \qquad (B.3)$$

$$\frac{1}{\lambda_{PS}} = \frac{3}{2}\frac{\langle(\hat{n}\cdot\nabla B)^2\rangle}{\langle B^2\rangle},$$

where

$$[A]_{mn} \equiv \frac{1}{(2\pi)^2} \int_0^{2\pi} \mathrm{d}\theta_B \int_0^{2\pi} \mathrm{d}\zeta_B A \exp\{-\mathrm{i}(m\theta_B + n\zeta_B)\}, \tag{B.4}$$

$\hat{n} \equiv \vec{B}/B$ and g_2 is the solution of the following deferential equation,

$$\vec{B} \cdot \nabla(\frac{g_2}{B^2}) = \vec{B} \times \nabla\psi \cdot \nabla(\frac{1}{B^2}), \tag{B.5}$$

with the condition $g_2(B = B_{max}) = 0$.

REFERENCES

[1] SHAING, K.C., CALLEN, J.D., Phys. Fluids **26** (1983) 3315.

[2] MURAKAMI, M., CARRERAS, B.A., BAYLOR, L.R., *et al.*, Phys. Rev. Lett. **66** (1991) 707. MURAKAMI, M., CARRERAS, B.A., BAYLOR, L.R., BELL, G.L., BIGELOW, T.S., ENGLAND, A.C., GLOWIENKA, J.C., HOWE, H.C., JERNIGAN, T.C., LEE, D.K., LYNCH, V.E., MA, C.H., RASMUSSEN, D.A., TOLLIVER, J.S., WADE, M.R., WILGEN, J.B., WING, W.R., Phys. Rev. Lett. **66** (1991) 707.

[3] RENNER, H., GASPARINO, U., MAASSBERG, H., *et al.*, in Plasma Physics and Controlled Nuclear Fusion Research 1990 (Proc. 13th Int. Conf. Washington DC, 1990), Vol.2, IAEA, Vienna (1991) 439.

[4] YAMADA, H., KUBO, S., WATANABE, K., *et al.*, Nuclear Fusion to be published.

[5] IIYOSHI, A., FUJIWARA, M., MOTOJIMA, O., OHYABU, N., YAMAZAKI, K., Fusion Technology **17** (1990) 169.

[6] WATANABE, K., NAKAJIMA, N., OKAMOTO, M., NAKAMURA, Y., WAKATANI, M., Nuclear Fusion **32** (1992) 1499.

[7] ICHIGUCHI, K., NAKAJIMA, N., OKAMOTO, M., NAKAMURA, Y., WAKATANI, M., Nuclear Fusion **33** (1993) 481.

[8] NAKAJIMA, N., OKAMOTO, M., J. Phys. Soc. Jpn. **61** (1992) 833.

[9] NAKAJIMA, N., OKAMOTO, M., FUJIWARA, M., J. Plasma and Fusion Res. **68** (1992) 503.

[10] SHAING, K.C., HIRSHMAN, S.P., CALLEN, J.D., Phys. Fluids **29** (1986) 521.

[11] HIRSHMAN, S.P., SIGMAR, D.J., Nuclear Fusion **21** (1981) 1079.

[12] SHAING, K.C., CARRERAS, B.A., DOMINGUEZ, N., LYNCH, V.E., TOLLIVER, J.S., Phys. Fluids **B1** (1989) 1663.

[13] HIRSHMAN, S.P., Phys. Fluids **26** (1983) 3553.

[14] HIRSHMAN, S.P., VAN RIJ, W.I., MERKEL, P., Comp. Phys. Commun. **43** (1986) 143.

[15] YAMAZAKI, K., KANEKO, H., TANIGUCHI, Y., *et al.*, Status of LHD Control System Design, National Institute for Fusion Science Report, NIFS-122, Dec. 1991.

[16] CORONAD, M., WOBIG, H., Phys. Fluids **29** (1986) 527.

FIGURE CAPTIONS

Fig.1 Radial profile of (a) bootstrap current density and (b) collisionality parameter $\bar{\nu}^*$ in low density case of $\langle n \rangle = 0.25 \times 10^{20}\mathrm{m}^{-3}$. Here $\bar{\nu}_i^* = \bar{\nu}_e^*$ since $T_i = T_e$, $\bar{\nu}^* << 1$ and $\bar{\nu}^* >> 1$ correspond to the $1/\nu$-regime limit and the plateau-regime limit, respectively. $\langle \beta \rangle \simeq 1.5\%$. In Fig.1(a), the solid line corresponds to the connection formula Eq.(1). Dashed line (almost overlapping with the solid line) and dotted-dashed line correspond to the $1/\nu$-regime limit and the plateau-regime limit, respectively. The density and temperature profiles are assumed as $n = n_0(1-s)$ and $T_i = T_e = T_0(1-s)$.

Fig.2 Radial profile of (a) bootstrap current density and (b) collisionality parameter $\bar{\nu}^*$ in high density case of $\langle n \rangle = 2.0 \times 10^{20}\mathrm{m}^{-3}$. $\langle \beta \rangle$ is same as Fig.1. Other parameters are also same as in Fig.1.

Fig.3 Dependence of (a) total bootstrap current and (b) collisionality parameter $\bar{\nu}^*$ at $\sqrt{s} \simeq 0.7$ on β value for three density (or collisionality) regimes. Circles, triangles and squares correspond to $\langle n \rangle = 0.25 \times 10^{20}\mathrm{m}^{-3}$, $\langle n \rangle = 1.0 \times 10^{20}\mathrm{m}^{-3}$ and $\langle n \rangle = 2.0 \times 10^{20}\mathrm{m}^{-3}$, respectively. The density and temperature profiles are assumed as $n = n_0(1-s)$ and $T_i = T_e = T_0(1-s)$.

Fig.4 Dependence of magnetic axis position for two density (or collisionality) cases on β value. Circles and squares correspond to $\langle n \rangle = 0.25 \times 10^{20}\mathrm{m}^{-3}$ and $\langle n \rangle = 2.0 \times 10^{20}\mathrm{m}^{-3}$, respectively. Closed rhombuses correspond to the currentless MHD equilibrium. Other parameters are the same as in Fig.3.

Fig.5 Rotational transform profile for (a) currentless case, (b) low density case $\langle n \rangle = 0.25 \times 10^{20}\mathrm{m}^{-3}$ and (c) high density case $\langle n \rangle = 2.0 \times 10^{20}\mathrm{m}^{-3}$ for various β values.

Fig.6 Well depth parameter profile for (a) currentless case, (b) low density case $\langle n \rangle = 0.25 \times 10^{20}\mathrm{m}^{-3}$ and (c) high density case $\langle n \rangle = 2.0 \times 10^{20}\mathrm{m}^{-3}$ for various β values.

Fig.7 Dependence of total bootstrap current on β value for various radial electric field. Circles, triangles and squares correspond to $\Phi = 0$, $\Phi = T_e$ and $\Phi = 2T_e$, respectively. Here $E_\psi = -\mathrm{d}\Phi/\mathrm{d}\psi$. The density and temperature profiles are $n = n_0(1-s)$ and $4T_i = T_e = T_0(1-s)$, respectively, $\langle n \rangle$ is fixed at $1.0 \times 10^{20}\mathrm{m}^{-3}$ and T_0 is varied.

Fig.8 Dependence of collisionality parameter $\bar{\nu}^*$ at $\sqrt{s} \simeq 0.7$ on β value. Open and closed circles correspond to ion and electron collisionality parameters, $\bar{\nu}_i^*$ and $\bar{\nu}_e^*$, where plasma parameters are the same in Fig.7, respectively. Open and closed squares

correspond to ion and electron collisionality parameters in the case of $T_{i0} = 0.5\text{keV}$, $T_{e0} = 4.5\text{keV}$, respectively, and $\langle n \rangle = 1.0 \times 10^{20}\text{m}^{-3}$.

Fig.9 Dependence of (a)total bootstrap current and (b) magnetic axis position on radial electric field at $\langle \beta \rangle \simeq 1.5\%$. Circles and squares correspond to the case of $T_{i0} = 1.0\text{keV}$, $T_{e0} = 4.0\text{keV}$ (small difference case between electron and ion collisionalities) and $T_{i0} = 0.5\text{keV}$, $T_{e0} = 4.5\text{keV}$ (large difference case between electron and ion collisionalities) for $\langle n \rangle = 1.0 \times 10^{20}\text{m}^{-3}$, respectively. In Fig.(b), dashed-dotted line correspond to the currentless MHD equilibrium. Here $\Phi_0 > 0$ and $\Phi_0 < 0$ correspond to $E_\psi > 0$ and $E_\psi < 0$, respectively.

Fig.10 Rotational transform profile in the case of $T_{i0} = 1.0\text{keV}$, $T_{e0} = 4.0\text{keV}$ (small difference case between electron and ion collisionalities) and $T_{i0} = 0.5\text{keV}$, $T_{e0} = 4.5\text{keV}$ (large difference case between electron and ion collisionalities) for $\langle n \rangle = 1.0 \times 10^{20}\text{m}^{-3}$, respectively.

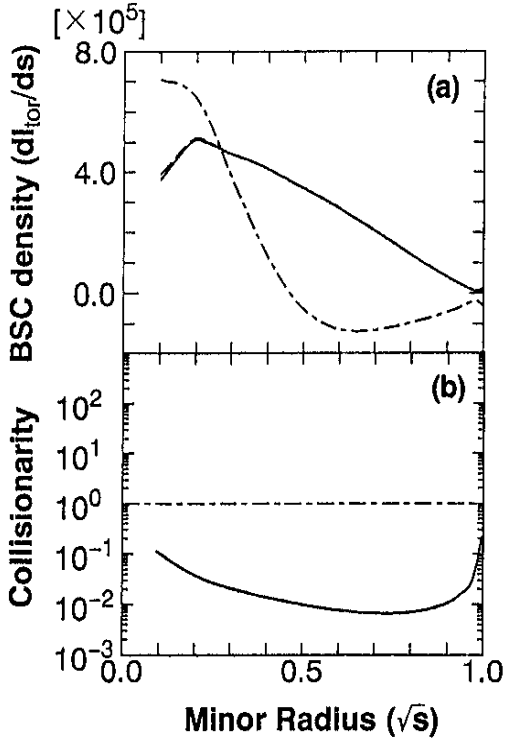

Fig.1
K.Y.Watanabe *et al.*

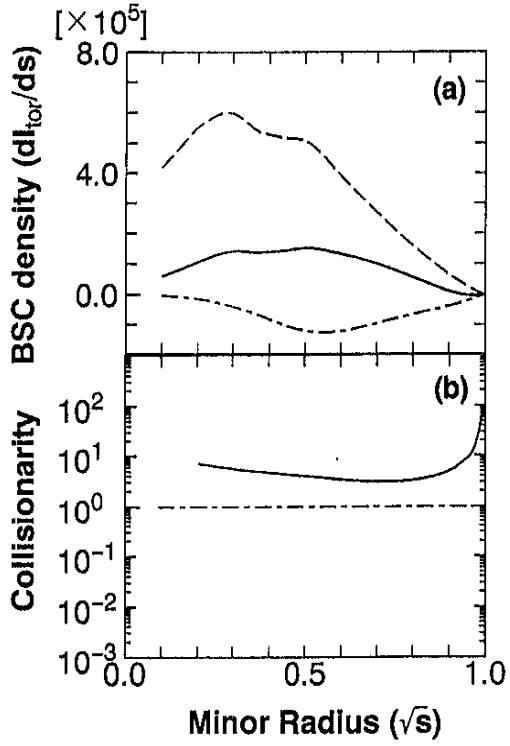

Fig.2
K.Y.Watanabe *et al.*

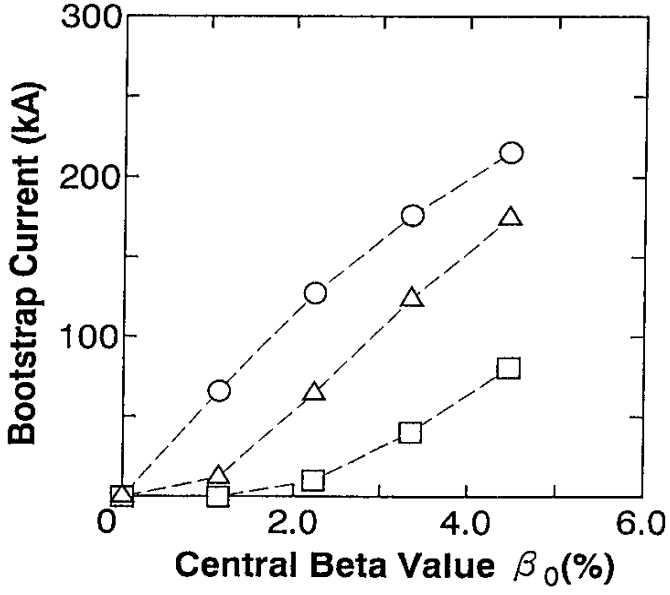

Fig.3(a)

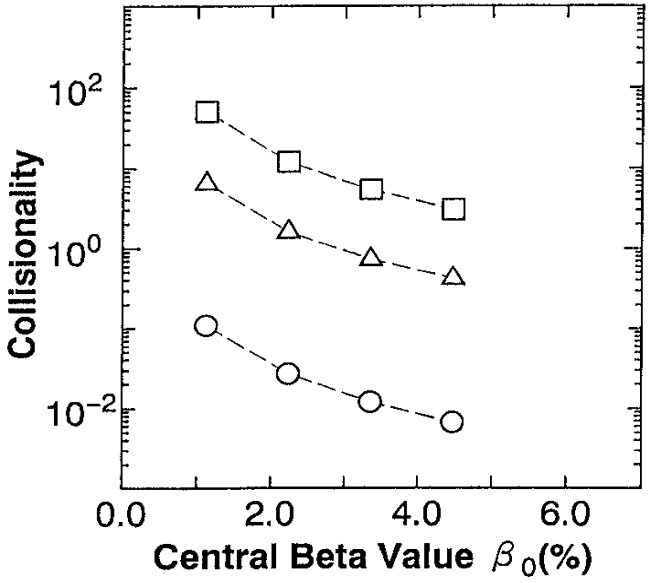

Fig.3(b)
K.Y.Watanabe *et al.*

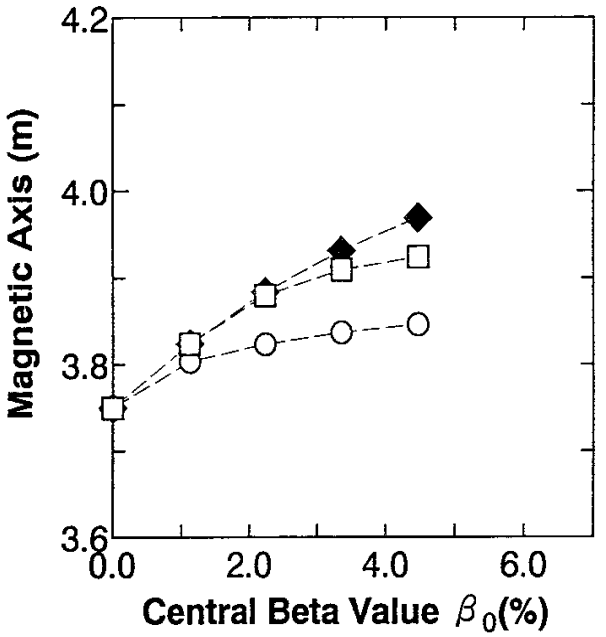

Fig.4
K.Y.Watanabe *et al.*

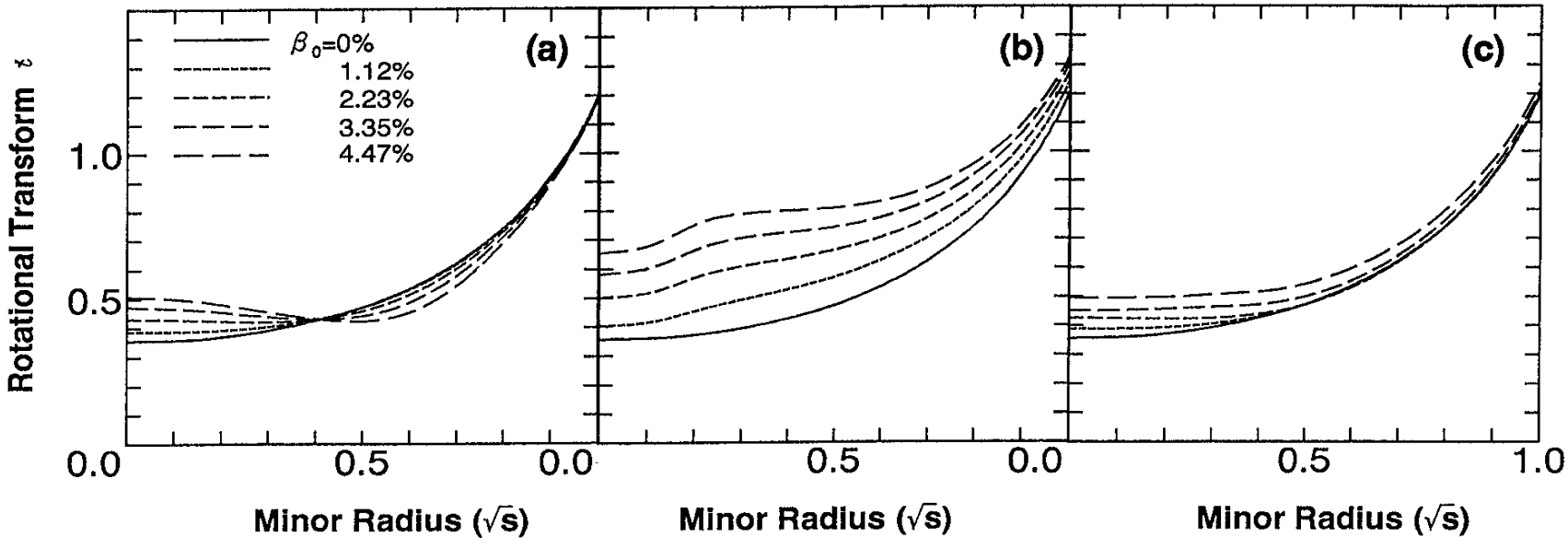

Fig.5
K.Y.Watanabe *et al.*

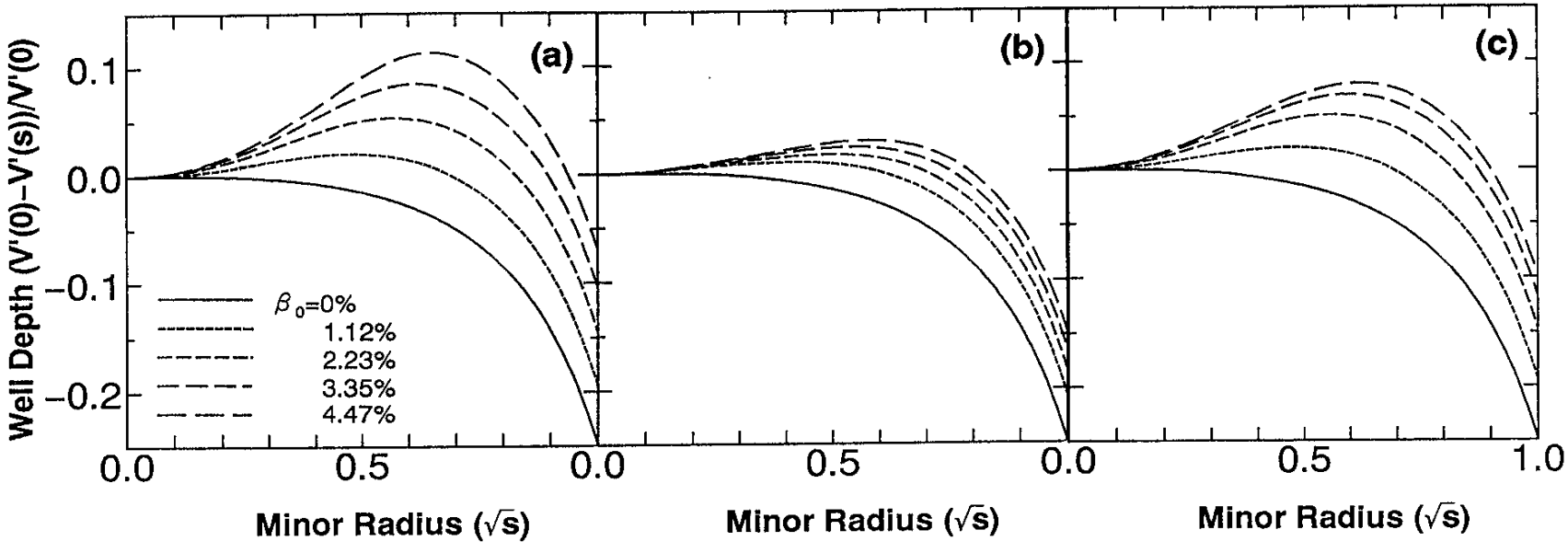

Fig.6
K.Y.Watanabe *et al.*

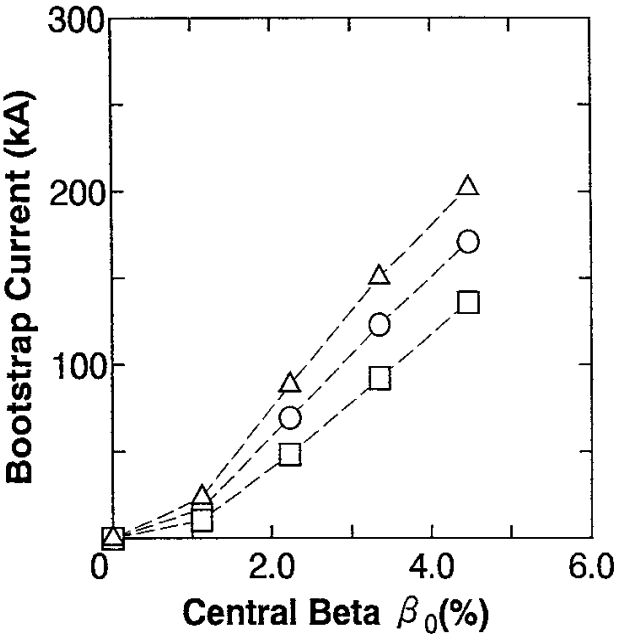

Fig.7
K.Y.Watanabe *et al.*

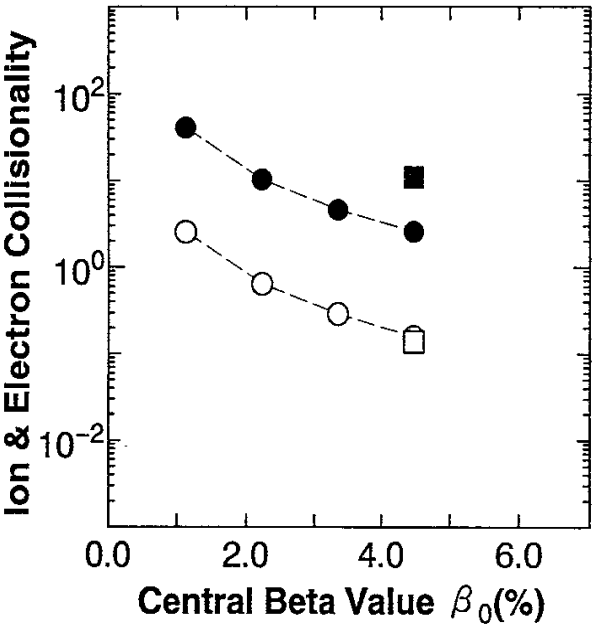

Fig.8
K.Y.Watanabe *et al.*

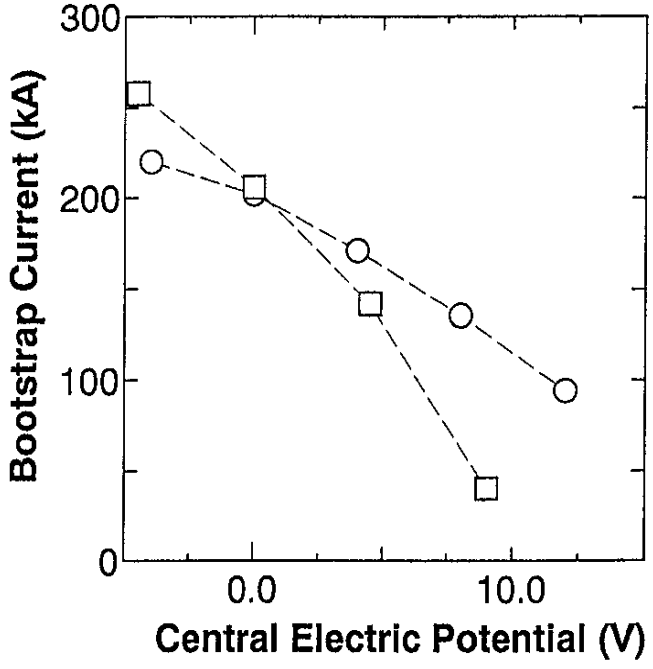

Fig.9(a)

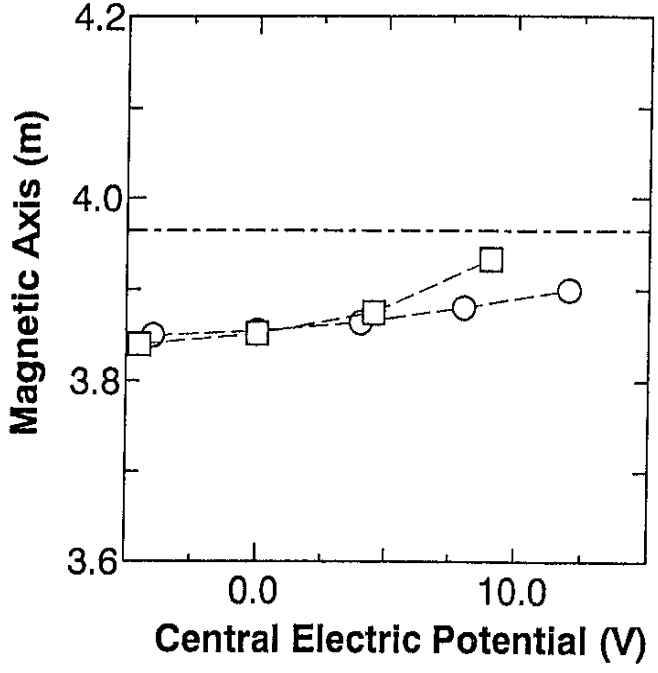

Fig.9(b)
K.Y.Watanabe *et al.*

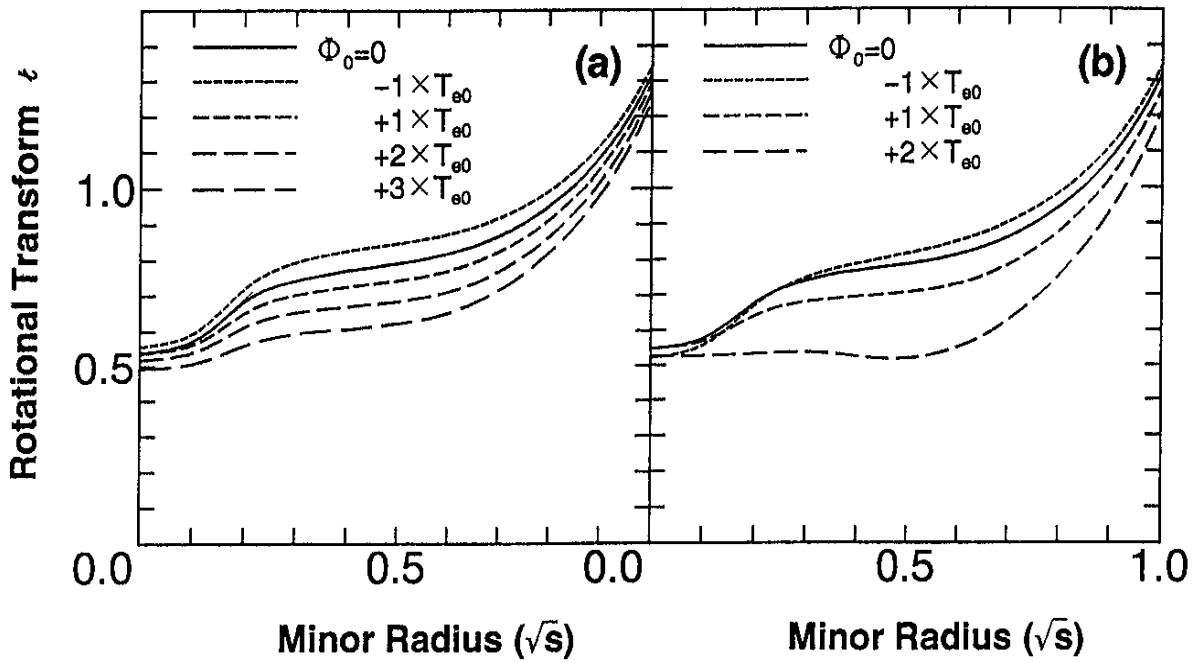

Fig.10
K.Y.Watanabe *et al.*

Recent Issues of NIFS Series

NIFS-240 Y. Miura, F. Okano, N. Suzuki, M. Mori, K. Hoshino, H. Maeda, T. Takizuka, JFT-2M Group, K. Itoh and S.-I. Itoh, *Ion Heat Pulse after Sawtooth Crash in the JFT-2M Tokamak;* Aug. 1993

NIFS-241 K. Ida, Y.Miura, T. Matsuda, K. Itoh and JFT-2M Group, *Observation of non Diffusive Term of Toroidal Momentum Transport in the JFT-2M Tokamak;* Aug. 1993

NIFS-242 O.J.W.F. Kardaun, S.-I. Itoh, K. Itoh and J.W.P.F. Kardaun, *Discriminant Analysis to Predict the Occurrence of ELMS in H-Mode Discharges;* Aug. 1993

NIFS-243 K. Itoh, S.-I. Itoh, A. Fukuyama, *Modelling of Transport Phenomena;* Sep. 1993

NIFS-244 J. Todoroki, *Averaged Resistive MHD Equations;* Sep. 1993

NIFS-245 M. Tanaka, *The Origin of Collisionless Dissipation in Magnetic Reconnection;* Sep. 1993

NIFS-246 M. Yagi, K. Itoh, S.-I. Itoh, A. Fukuyama and M. Azumi, *Current Diffusive Ballooning Mode in Seecond Stability Region of Tokamaks;* Sep. 1993

NIFS-247 T. Yamagishi, *Trapped Electron Instabilities due to Electron Temperature Gradient and Anomalous Transport;* Oct. 1993

NIFS-248 Y. Kondoh, *Attractors of Dissipative Structure in Three Disspative Fluids;* Oct. 1993

NIFS-249 S. Murakami, M. Okamoto, N. Nakajima, M. Ohnishi, H. Okada, *Monte Carlo Simulation Study of the ICRF Minority Heating in the Large Helical Device;* Oct. 1993

NIFS-250 A. Iiyoshi, H. Momota, O. Motojima, M. Okamoto, S. Sudo, Y. Tomita, S. Yamaguchi, M. Ohnishi, M. Onozuka, C. Uenosono, *Innovative Energy Production in Fusion Reactors*; Oct. 1993

NIFS-251 H. Momota, O. Motojima, M. Okamoto, S. Sudo, Y. Tomita, S. Yamaguchi, A. Iiyoshi, M. Onozuka, M. Ohnishi, C. Uenosono, *Characteristics of D-^{3}He Fueled FRC Reactor: ARTEMIS-L,* Nov. 1993

NIFS-252 Y. Tomita, L.Y. Shu, H. Momota,
Direct Energy Conversion System for D-^{3}He Fusion, Nov. 1993

NIFS-253 S. Sudo, Y. Tomita, S. Yamaguchi, A. Iiyoshi, H. Momota, O. Motojima, M. Okamoto, M. Ohnishi, M. Onozuka, C. Uenosono,
Hydrogen Production in Fusion Reactors, Nov. 1993

NIFS-254 S. Yamaguchi, A. Iiyoshi, O. Motojima, M. Okamoto, S. Sudo, M. Ohnishi, M. Onozuka, C. Uenosono,
Direct Energy Conversion of Radiation Energy in Fusion Reactor, Nov. 1993

NIFS-255 S. Sudo, M. Kanno, H. Kaneko, S. Saka, T. Shirai, T. Baba,
Proposed High Speed Pellet Injection System "HIPEL" for Large Helical Device
Nov. 1993

NIFS-256 S. Yamada, H. Chikaraishi, S. Tanahashi, T. Mito, K. Takahata, N. Yanagi, M. Sakamoto, A. Nishimura, O. Motojima, J. Yamamoto, Y. Yonenaga, R. Watanabe,
Improvement of a High Current DC Power Supply System for Testing the Large Scaled Superconducting Cables and Magnets; Nov. 1993

NIFS-257 S. Sasaki, Y. Uesugi, S. Takamura, H. Sanuki, K. Kadota,
Temporal Behavior of the Electron Density Profile During Limiter Biasing in the HYBTOK-II Tokamak; Nov. 1993

NIFS-258 K. Yamazaki, H. Kaneko, S. Yamaguchi, K.Y. Watanabe, Y.Taniguchi, O.Motojima, LHD Group,
Design of Central Control System for Large Helical Device (LHD); Nov. 1993

NIFS-259 S. Yamada, T. Mito, A. Nishimura, K. Takahata, S. Satoh, J. Yamamoto, H. Yamamura, K. Masuda, S. Kashihara, K. Fukusada, E. Tada,
Reduction of Hydrocarbon Impurities in 200L/H Helium Liquefier-Refrigerator System; Nov. 1993

NIFS-260 B.V.Kuteev,
Pellet Ablation in Large Helical Device; Nov. 1993

NIFS-261 K. Yamazaki,
Proposal of "MODULAR HELIOTRON': Advanced Modular Helical System Compatible with Closed Helical Divertor; Nov. 1993

NIFS-262 V.D.Pustovitov,
Some Theoretical Problems of Magnetic Diagnostics in Tokamaks and Stellarators; Dec. 1993

NIFS-263 A. Fujisawa, H. Iguchi, Y. Hamada

A Study of Non-Ideal Focus Properties of 30° Parallel Plate Energy Analyzers; Dec. 1993

NIFS-264 K. Masai,
Nonequilibria in Thermal Emission from Supernova Remnants; Dec. 1993

NIFS-265 K. Masai, K. Nomoto,
X-Ray Enhancement of SN 1987A Due to Interaction with its Ring-like Nebula; Dec. 1993

NIFS-266 J. Uramoto
A Research of Possibility for Negative Muon Production by a Low Energy Electron Beam Accompanying Ion Beam; Dec. 1993

NIFS-267 H. Iguchi, K. Ida, H. Yamada, K. Itoh, S.-I. Itoh, K. Matsuoka, S. Okamura, H. Sanuki, I. Yamada, H. Takenaga, K. Uchino, K. Muraoka,
The Effect of Magnetic Field Configuration on Particle Pinch Velocity in Compact Helical System (CHS); Jan. 1994

NIFS-268 T. Shikama, C. Namba, M. Kosuda, Y. Maeda,
Development of High Time-Resolution Laser Flash Equipment for Thermal Diffusivity Measurements Usting Miniature-Size Specimens; Jan. 1994

NIFS-269 T. Hayashi, T. Sato, P. Merkel, J. Nührenberg, U. Schwenn,
Formation and 'Self-Healing' of Magnetic Islands in Finite-β Helias Equilibria; Jan. 1994

NIFS-270 S. Murakami, M. Okamoto, N. Nakajima, T. Mutoh,
Efficiencies of the ICRF Minority Heating in the CHS and LHD Plasmas; Jan. 1994

NIFS-271 Y. Nejoh, H. Sanuki,
Large Amplitude Langmuir and Ion-Acoustic Waves in a Relativistic Two-Fluid Plasma; Feb. 1994

NIFS-272 A. Fujisawa, H. Iguchi, A. Taniike, M. Sasao, Y. Hamada,
A 6MeV Heavy Ion Beam Probe for the Large Helical Device; Feb. 1994

NIFS-273 Y. Hamada, A. Nishizawa, Y. Kawasumi, K. Narihara, K. Sato, T. Seki, K. Toi, H. Iguchi, A. Fujisawa, K. Adachi, A. Ejiri, S. Hidekuma, S. Hirokura, K. Ida, J. Koong, K. Kawahata, M. Kojima, R. Kumazawa, H. Kuramoto, R. Liang, H. Sakakita, M. Sasao, K. N. Sato, T. Tsuzuki, J. Xu, I. Yamada, T. Watari, I. Negi,
Measurement of Profiles of the Space Potential in JIPP T-IIU Tokamak Plasmas by Slow Poloidal and Fast Toroidal Sweeps of a

Heavy Ion Beam; Feb. 1994

NIFS-274 M. Tanaka,
A Mechanism of Collisionless Magnetic Reconnection; Mar. 1994

NIFS-275 A. Fukuyama, K. Itoh, S.-I. Itoh, M. Yagi and M. Azumi,
Isotope Effect on Confinement in DT Plasmas; Mar. 1994

NIFS-276 R.V. Reddy, K. Watanabe, T. Sato and T.H. Watanabe,
Impulsive Alfven Coupling between the Magnetosphere and Ionosphere; Apr.1994

NIFS-277 J. Uramoto,
A Possibility of π^- Meson Production by a Low Energy Electron Bunch and Positive Ion Bunch; Apr. 1994

NIFS-278 K. Itoh, S.-I. Itoh, A. Fukuyama, M. Yagi and M. Azumi,
Self-sustained Turbulence and L-mode Confinement in Toroidal Plasmas II; Apr. 1994

NIFS-279 K. Yamazaki and K.Y.Watanabe,
New Modular Heliotron System Compatible with Closed Helical Divertor and Good Plasma Confinement; Apr. 1994

NIFS-280 S. Okamura, K. Matsuoka, K. Nishimura, K. Tsumori, R. Akiyama, S. Sakakibara, H. Yamada, S. Morita, T. Morisaki,. N. Nakajima, K. Tanaka, J. Xu, K. Ida, H. Iguchi, A. Lazaros, T. Ozaki, H. Arimoto, A. Ejiri, M. Fujiwara, H. Idei. O. Kaneko, K. Kawahata, T. Kawamoto, A. Komori, S. Kubo, O. Motojima, V.D. Pustovitov, C. Takahashi, K. Toi and I. Yamada,
High-Beta Discharges with Neutral Beam Injection in CHS, Apr; 1994

NIFS-281 K. Kamada, H. Kinoshita and H. Takahashi,
Anomalous Heat Evolution of Deuteron Implanted Al on Electron Bombardment ; May 1994

NIFS-282 H. Takamaru, T. Sato, K. Watanabe and R. Horiuchi,
Super Ion Acoustic Double Layer; May 1994

NIFS-283 O.Mitarai and S. Sudo
Ignition Characteristics in D-T Helical Reactors; June 1994

NIFS-284 R. Horiuchi and T. Sato,
Particle Simulation Study of Driven Magnetic Reconnection in a Collisionless Plasma; June 1994